Pharm Res (2012) 29:2249–2263
DOI 10.1007/s11095-012-0753-1

RESEARCH PAPER

Chloroquine-Mediated Lysosomal Dysfunction Enhances the Anticancer Effect of Nutrient Deprivation

Ljubica Harhaji-Trajkovic • Katarina Arsikin • Tamara Kravic-Stevovic • Sasa Petricevic • Gordana Tovilovic • Aleksandar Pantovic • Nevena Zogovic • Biljana Ristic • Kristina Janjetovic • Vladimir Bumbasirevic • Vladimir Trajkovic

Received: 1 February 2012 / Accepted: 2 April 2012 / Published online: 27 April 2012

ABSTRACT

Purpose To investigate the ability of chloroquine, a lysosomotropic autophagy inhibitor, to enhance the anticancer effect of nutrient deprivation.

Methods Serum-deprived U251 glioma, B16 melanoma and L929 fibrosarcoma cells were treated with chloroquine *in vitro*. Cell viability was measured by crystal violet and MTT assay. Oxidative stress, apoptosis/necrosis and intracellular acidification were analyzed by flow cytometry. Cell morphology was examined by light and electron microscopy. Activation of AMP-activated protein kinase (AMPK) and autophagy were monitored by immunoblotting. RNA interference was used for AMPK and LC3b knockdown. The anticancer efficiency of intraperitoneal chloroquine in calorie-restricted mice was assessed using a B16 mouse melanoma model.

Results Chloroquine rapidly killed serum-starved cancer cells *in vitro*. This effect was not mimicked by autophagy inhibitors or LC3b shRNA, indicating autophagy-independent mechanism. Chloroquine-induced lysosomal accumulation and oxidative stress, leading to mitochondrial depolarization, caspase activation and mixed apoptotic/necrotic cell death, were prevented by lysosomal acidification inhibitor bafilomycin. AMPK downregulation participated in chloroquine action, as AMPK activation reduced, and AMPK shRNA mimicked chloroquine toxicity. Chloroquine inhibited melanoma growth in calorie-restricted mice, causing lysosomal accumulation, mitochondrial disintegration and selective necrosis of tumor cells.

Conclusion Combined treatment with chloroquine and calorie restriction might be useful in cancer therapy.

KEY WORDS AMPK · autophagy · caloric restriction · cancer · chloroquine

ABBREVIATIONS

AICAR	5-aminoimidazole-4-carboxamide riboside
AMPK	AMP-activated protein kinase
DHR	dihydrorhodamine
FCS	fetal calf serum
FITC	fluorescein isothyocyanate
LC3	microtubule-associated protein 1 light-chain 3
MEM	Eagle's Minimum Essential Medium
MTT	3-(4,5-dimethylthiazol-2-yl)-2,5-diphenyltetrazolium bromide
PBS	phosphate buffered saline
PI	propidium iodide
ROS	reactive oxygen species
shRNA	short hairpin RNA

INTRODUCTION

Calorie restriction has been shown to increase lifespan and to reduce the incidence of various diseases, including cancer (1,2). Numerous studies have demonstrated that calorie restriction inhibits both carcinogenesis and tumor growth through a decrease in concentration of growth factors and other mechanisms leading to proliferation arrest and

Ljubica Harhaji-Trajkovic and Katarina Arsikin contributed equally to the work.

L. Harhaji-Trajkovic (✉) · G. Tovilovic · N. Zogovic · K. Janjetovic
Institute for Biological Research, University of Belgrade
Despot Stefan Blvd. 142, 11060 Belgrade, Serbia
e-mail: buajk@yahoo.com

K. Arsikin · A. Pantovic · B. Ristic · K. Janjetovic · V. Trajkovic (✉)
Institute of Microbiology and Immunology, School of Medicine
University of Belgrade
Dr. Subotica 1, 11000 Belgrade, Serbia
e-mail: vtrajkovic@med.bg.ac.rs

T. Kravic-Stevovic · V. Bumbasirevic
Institute of Histology and Embryology, School of Medicine
University of Belgrade
Belgrade, Serbia

S. Petricevic
Institute of Biomedical Research, Galenika a.d.
Belgrade, Serbia

subsequent apoptotic cell death (3,4). In order to survive until the supply of nutrients is restored, cells inhibit protein synthesis and mount autophagy, a process in which cytoplasmic content is sequestered in double-membrane vesicles (autophagosomes) and targeted for degradation following the fusion with lysosomes and formation of autophagolysosomes (5). The role of autophagy in nutrient-deprived cells is to digest damaged proteins and organelles, recycling fatty acids and amino acids for synthesis of crucial macromolecules or for oxidation in mitochondria necessary to maintain ATP level for essential cell metabolism (6). Therefore, autophagy acts as a survival mechanism against metabolic stress, and inhibition of autophagy facilitates cell death during hypoxia or growth factor and nutrient deprivation (7,8). Being less able to metabolize ketone bodies and fat, cancer cells are mainly dependent on glucose presence and consequently more sensitive to nutrient deprivation than normal cells (9). Accordingly, combination of caloric restriction and autophagy inhibition represents a valid therapeutic strategy in cancer treatment (10,11).

Chloroquine, a worldwide used antimalaric and anti-inflammatory drug with autophagy-inhibiting properties, is the most appropriate candidate for therapeutic inhibition of autophagy, due to the feasibility of its introduction to the clinical settings of cancer therapy without need of animal or phase-one studies. It inhibits proliferation and/or induces cell death in various cancer cell lines (12–17) and potentiates the anticancer effect of ionizing radiation and chemotherapeutic agents such as Akt inhibitors (18,19). Chloroquine is a lysosomotropic drug that raises intralysosomal pH (20) and impairs autophagic protein degradation (21), which leads to the accumulation of ineffective autophagosomes and cell death in nutrient-deprived bone marrow cells reliant on autophagy for survival (22) or proteasome inhibitor-treated breast cancer cells (23). However, the possible autophagy-independent mechanisms of chloroquine-mediated sensitization of cancer cells to nutrient deprivation, as well as the combined effect of chloroquine and classic calorie restriction on tumor progression *in vivo* have not been investigated.

In the present study, we describe the ability of chloroquine to potentiate nutrient deprivation-induced killing of various cancer cell lines. The observed effect did not rely solely on autophagy inhibition and involved lysosomal damage-dependent apoptotic and necrotic cell death. Moreover, chloroquine synergized with caloric restriction in reducing melanoma growth *in vivo*.

MATERIALS AND METHODS

Cells and Reagents

All reagents were purchased from Sigma (St. Louis, MO), unless stated otherwise. The human glioma cell line U251 was kindly donated by Dr. Pedro Tranque (Universidad de Castilla-La Mancha, Albacete, Spain), while the mouse B16 melanoma cell line and the mouse fibrosarcoma cell line L929 were obtained from the European Collection of Animal Cell Cultures (Salisbury, UK). The tumor cell lines were maintained at 37 °C in a humidified atmosphere with 5 % CO_2, in a MEM cell culture medium (PAA Laboratories, Pasching, Austria) supplemented with 5 % fetal calf serum (FCS) and penicillin/streptomycin. The cells were prepared for experiments using the conventional trypsinization procedure with trypsin/EDTA and incubated in 96-well flat-bottom plates (1×10^4 cells/well) for the cell viability assessment, 24-well plates (5×10^4 cells/well) for the flow cytometric analysis, or 60 mm Petri dishes (1×10^6 cells) for the Western blotting. Cells were rested for 24 h in cell culture medium with FCS and then treated with chloroquine (chloroquine diphosphate salt) in MEM with or without FCS ("standard" and "starvation" medium, respectively), in the absence or presence of the antioxidants N-acetylcysteine and butylated hydroxyanisole, inhibitor of mitochondrial transition pore opening cyclosporine A, AMPK activator 5-aminoimidazole-4-carboxamide riboside (AICAR), or the autophagy inhibitors wortmannin, bafilomycin-A1 and NH_4Cl, as described in Results and Figure legends.

Determination of Cell Number and Cellular Respiration

The cell number and cellular respiration as a marker of cell viability were determined exactly as previously described, using crystal violet to stain viable, adherent cells and MTT assay to measure the activity of mitochondrial dehydrogenases (24). The crystal violet or MTT absorbance, corresponding to the number of viable cells or their mitochondrial dehydrogenase activity, respectively, was measured in an automated microplate reader at 570 nm. The results were presented as % of the control value obtained in untreated cells.

DNA Fragmentation and Apoptosis/Necrosis Analysis

DNA fragmentation was analyzed by flow cytometry using a DNA-binding dye propidium iodide (PI) as previously described (24). Apoptotic/necrotic cell death was analyzed by flow cytometry following double staining with annexin V-FITC and PI, in which annexin V binds to apoptotic cells with exposed phosphatidylserine, while PI labels the necrotic cells with membrane damage. Staining was performed according to the instructions by the manufacturer (BD Pharmingen, San Diego, CA). A green/red (FL1/FL2) fluorescence of annexin/PI^- and PI-stained cells was analyzed with FACSCalibur flow cytometer (BD, Heidelberg,

Germany), using a peak fluorescence gate to exclude cell aggregates during cell cycle analysis. The numbers of viable (annexin$^-$/PI$^-$), apoptotic (annexin$^+$/PI$^-$) and necrotic (annexin$^+$/PI$^+$) cells, as well as the proportion of hypodyploid, apoptotic cells with fragmented DNA (sub-G compartment) were determined using a Cell Quest Pro software (BD).

Caspase Activation

Activation of caspases was measured by flow cytometry after labeling the cells with a cell-permeable, FITC-conjugated pan-caspase inhibitor (ApoStat; R&D Systems, Minneapolis, MN) according to the manufacturer's instructions. The increase in green fluorescence (FL-1) as a measure of caspase activity within individual cells of the treated population was determined using FACSCalibur flow cytometer. The results are expressed as % of cells containing active caspases.

Measurement of Mitochondrial Membrane Potential and Reactive Oxygen Species (ROS)

Mitochondrial membrane potential was assessed using DePsipher (R&D Systems, Minneapolis, MN), a lipophilic cation that has the property of aggregating upon membrane polarization forming an orange-red fluorescent compound. If the potential is disturbed, the dye cannot access the transmembrane space and remains or reverts to its green monomeric form. The cells were stained with DePsipher as described by the manufacturer, and the green monomer and the red aggregates were detected by flow cytometry. The results were presented as a green/red fluorescence ratio (FL1/FL2, arbitrarily set to 1 in control samples), the increase and decrease of which reflect mitochondrial depolarization and hyperpolarization, respectively. Intracellular production of ROS was quantified by flow cytometric analysis of the green fluorescence (FL1) emitted by redox-sensitive dye dihydrorhodamine 123 (DHR; Invitrogen, Paisley, UK), as previously described (25) .

Detection of Acidic Intracellular Vesicles

The acidic vesicles (i.e. lysosomes, autophagolysosomes) were visualized by supravital acridine orange staining. After incubation, cells were washed with PBS and stained with acridine orange (1 μM; Sigma, St. Louis, MO) for 15 min. at 37 °C. Subsequently, cells were washed and analyzed under the inverted fluorescent microscope (Leica Microsystems DMIL, Wetzlar, Germany) using Leica Microsystems DFC320 camera and Leica Application Suite software (version 2.8.1). Depending on their acidity, autophagolysosomes and lysosomes appeared as orange/red fluorescent cytoplasmic vesicles, while nuclei were stained green. Alternatively, acridine orange-stained cells were trypsinized, washed and analyzed on a FACSCalibur flow cytometer using Cell Quest Pro software. Accumulation of acidic vesicles was quantified as red/green fluorescence ratio (mean FL3/FL1).

Immunoblotting

Cells were lysed in lysis buffer (30 mM Tris–HCl pH 8.0, 150 mM NaCl, 1 % NP-40, 1 mM phenylmethylsulfonyl-fluoride and protease inhibitor cocktail) on ice for 30 min, centrifuged at 14000 g for 15 min at 4 °C, and the supernatants were collected. Equal amounts of protein from each sample were separated by SDS-PAGE and transferred to nitrocellulose membranes (Bio-Rad, Marnes-la-Coquette, France). Following incubation with antibodies against microtubule-associated protein 1 light-chain 3 (LC3), p62, phospho-AMP-activated protein kinase (AMPK), AMPK and actin (Cell Signaling Technology, Beverly, MA) as primary antibodies and peroxidase-conjugated goat anti-rabbit IgG (Jackson IP Laboratories, West Grove, PA) as a secondary antibody, specific protein bands were visualized using enhanced chemiluminescence reagents for Western blot analysis (Amersham Pharmacia Biotech, Piscataway, NJ). The signal intensity was determined by densitometry and the results were presented as relative to control value, which was arbitrarily set to 1.

Transfection with Short Hairpin RNA (shRNA)

The shRNA targeting human LC3b or AMPKalpha1/2 genes, as well as scrambled control shRNA were obtained from Santa Cruz Biotechnology (Santa Cruz, CA). Subconfluent U251 in 6 well plates were transfected with LC3b, AMPK or control shRNA according to the manufacturer's protocol, using shRNA Plasmid Transfection Reagent and Medium (Santa Cruz Biotechnology, Santa Cruz, CA). The stably transfected cells were selected as recommended by manufacturer and maintained in selection medium containing puromycin (10 μg/ml).

Transmission Electron Microscopy (TEM)

Trypsinized tumor cells or tumor tissue sections were fixed in 3 % glutaraldehyde, postfixed in 1 % osmium tetroxide, dehydrated in graded alcohols and then embedded in Epon 812. The ultrathin sections were stained in uranyl acetate and lead citrate and were examined using a Morgagni 268D electron microscope (FEI, Hillsboro, OR).

Induction of Melanoma in C57Bl/6 Mice and Treatment Regimen

Primary tumors were induced by subcutaneous injection of 3×10^5 B16 melanoma cells in the dorsal lumbosacral region of syngeneic 5–6 weeks-old female C57Bl/6 mice (Institute for Biological Research, Belgrade, Serbia). The mice (n=32) were kept under a 12:12 h light–dark cycle, at 22±2 °C, and were accustomed to daily handling. They received standard balanced diet for laboratory mice (D. D. Veterinarski zavod Subotica, Subotica, Serbia) and water *ad libitum*. Five days after tumor implantation all animals were randomly divided into four groups (n=8 per group): 1. control (normally fed, receiving daily i.p. PBS), 2. chloroquine (normally fed, receiving daily i.p. 20 mg/kg of chloroquine), 3. caloric restriction (fed with 70 % of their normal food intake, receiving daily i.p. PBS) and 4. chloroquine + caloric restriction (calorie-restricted mice receiving daily i.p. 20 mg/kg of chloroquine). Tumor growth was monitored every 2 to 3 days by two-dimensional measurements of individual tumors for each mouse. Tumor volume (cm^3) was calculated according to the formula: $(\pi/6)\times$tumor length$\times$ tumor width^2. At the end of the experiment (day 20 after tumor implantation), the animals were sacrificed. Tumors, hearts, kidneys and livers were excised, fixed in 4 % formalin solution and embedded in paraffin. Serial tissue sections (4 μm thick) were deparaffinized in xylol and serial alcohol, and were later used for hemathoxilin-eosin staining. Tumor sections were also stained with Sudan black B, for 30 min at room temperature, for detection of lipids. Sudan black B stained sections were counterstained with Neutral Red. Digital images of hemathoxilin-eosin- and Sudan black B-stained sections were made on an Olympus BX41TF light microscope equipped with a digital camera. All animal experiments were approved by the Local Animal Care Committee and conformed to the ethical guidelines stated in the "Principles of Laboratory Animal Care" (NIH publication #85-23, revised in 1985).

Statistical Analysis

The statistical significance of the differences was analyzed by t-test or ANOVA followed by the Student-Newman-Keuls test. The efficacy of *in vivo* treatments was evaluated by Mann–Whitney U test. A P value of less than 0.05 was considered statistically significant.

RESULTS

Chloroquine Decreases Viability of FCS-Deprived U251 Glioma Cells

Deprivation of serum from cultivation medium has been used as an *in vitro* model for calorie restriction (26,27). Treatment with chloroquine (5–20 μM) alone for 24 h in medium with FCS was not toxic to U251 glioma cell line, as confirmed by both crystal violet and MTT assay (Fig. 1a). On the other hand, chloroquine in a dose-dependent manner potentiated the reduction in cell numbers and mitochondrial dehydrogenase activity in FCS-deprived cells (Fig. 1a). Both FCS deprivation and chloroquine increased intracellular levels of autophagosome-associated LC3-II (Fig. 1b), reflecting the induction of autophagy by starvation and inhibition of autophagic LC3-II proteolysis by chloroquine. Accordingly, the concentration of the selective autophagic target p62 (28) was reduced by FCS depletion, but markedly increased by chloroquine both in the presence and absence of FCS (Fig. 1b), confirming its ability to block autophagic proteolysis. However, both early (wortmannin) and late (bafilomycin A1, NH_4Cl) autophagy inhibitors, which prevent PI3 kinase class III-dependent autophagosome formation and autophagolysosome acidification, respectively (29–31), failed to mimic chloroquine-mediated potentiation of FCS deprivation-induced toxicity towards U251 glioma (Fig. 1c, d). The observed absence of cytotoxicity was not due to ineffective inhibition of autophagy, as flow cytometric analysis of cells stained with a pH-sensitive dye acridine orange confirmed that all investigated compounds significantly reduced starvation-triggered intracellular acidification as one of the autophagy hallmarks (Fig. 1e). Furthermore, U251 cells transfected with shRNA against autophagy-essential LC3b were not more sensitive to starvation than control cells, and chloroquine was equally toxic to both LC3b-deficient and control tumor cells (Fig. 1f; the insert shows immunoblot confirmation of LC3b knockdown). It should be noted that the cytotoxic effects of autophagy inhibition with LC3b shRNA, although not apparent

Fig. 1 Chloroquine decreases viability of FCS-depleted cancer cells independently of autophagy inhibition. (**a**) U251 cells were incubated in medium with or without FCS, in the presence of different doses of chloroquine (CQ) and cell viability was assessed after 24 h by MTT or crystal violet (CV) test. (**b**) U251 cells were incubated in medium with or without FCS, in the absence or presence of chloroquine (20 μM). Immunoblot analysis of LC3, p62 and actin was performed after 8 h and representative immunoblots are presented. (**c**–**e**) U251 cells were incubated in medium with or without FCS, in the absence or presence of chloroquine (20 μM), bafilomycin A1 (BAF; 2 nM), NH_4Cl (25 mM) or wortmannin (WMN; 100 nM). After 24 h, cell viability was assessed by MTT (**c**) or crystal violet test (**d**), while the presence of acidic vesicles in acridine orange-stained cells was evaluated by flow cytometry ((**e**) the insert shows the representative histograms). (**f**) U251 cells transfected with control or LC3b shRNA were incubated in FCS-free medium without or with chloroquine (20 μM) and cell viability was determined after 24 h by MTT or CV assay (the insert shows immunoblot analysis of LC3b in cells transfected with control or LC3b shRNA). The data are mean ± SD values of triplicates from a representative of three experiments (**a**, **c**, **d**, **f**) or mean ± SD values from three independent experiments (**e**) ($^{\#}p<0.05$ or $^{*}p<0.05$ refer to cells in medium with or without FCS, respectively).

after 24 h (Fig. 1f), were clearly visible after prolonged incubation (48 h) in nutrient-deficient medium (25.7 ± 2.3 *vs.* 15.4 ± 0.4 % viability in control shRNA and LC3 shRNA-transfected U251 cells, respectively; $P<0.05$). Collectively,

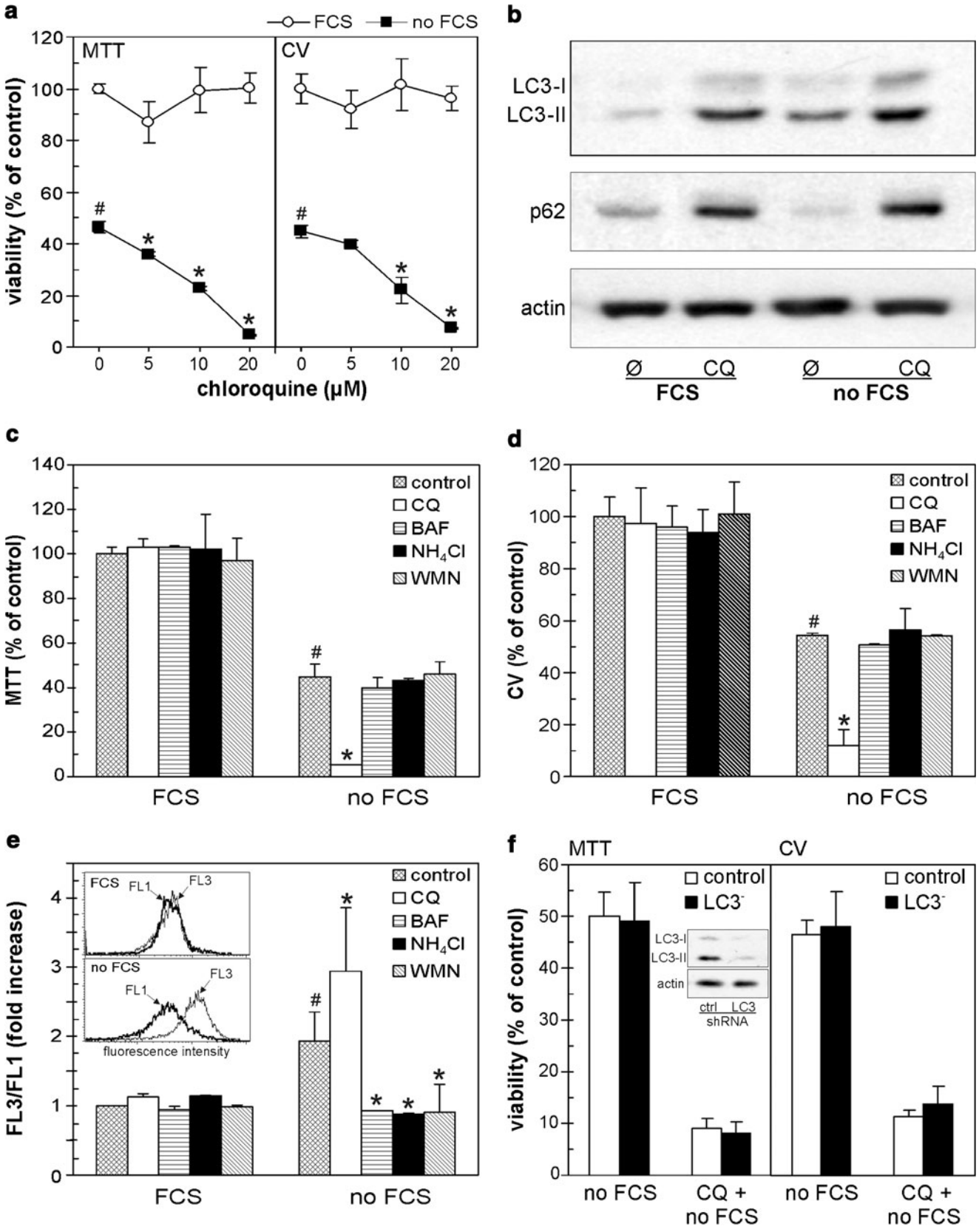

these data demonstrate that the rapid *in vitro* killing of nutrient-deprived glioma cells by chloroquine is not mediated solely by autophagy inhibition.

Chloroquine Induces Oxidative Stress- and Mitochondrial Depolarization-Mediated Apoptosis and Necrosis in FCS-Deprived U251 Cells

We next explored the mechanism responsible for the synergistic *in vitro* anticancer action of chloroquine and nutrient deprivation. Flow cytometric analysis of phosphatidylserine externalization (Annexin-FITC) and membrane permeabilization (PI) as the respective markers of apoptosis and necrosis, revealed that chloroquine alone was without any effect, while FCS depletion induced only marginal increase in numbers of apoptotic and necrotic cells (Fig. 2a). However, incubation of FCS-deprived U251 cells with chloroquine significantly increased apoptotic and necrotic cell death (Fig. 2a). Both apoptosis and necrosis were detected simultaneously starting from 12 h treatment onward, suggesting that this early necrotic cell death was genuine and not secondary to apoptosis (Fig. 2f). The moderate increase in DNA fragmentation and activation of caspases, the apoptosis-executing enzymes, observed in FCS-starved cells, was also markedly augmented by concomitant addition of chloroquine (Fig. 2b, c). The combination of FCS withdrawal and chloroquine treatment triggered oxidative stress and mitochondrial membrane depolarization in U251 cells, as demonstrated respectively by an increase in redox-sensitive DHR fluorescence (Fig. 2d) and a green-to-red (FL1-FL2) fluorescence shift of the mitochondria-binding dye DePsipher (Fig. 2e). The loss of mitochondrial membrane potential lagged after ROS production, suggesting that mitochondrial depolarization might be a consequence of oxidative stress (Fig. 2g, h). The involvement of oxidative stress and mitochondrial depolarization in chloroquine-induced death of FCS-deprived tumor cell was confirmed using the antioxidants N-acetylcysteine or butylated hydroxyanisole and the inhibitor of mitochondrial transition pore opening cyclosporine A, which all improved cell survival to a certain extent (Fig. 2i). Therefore, it appears that combination of nutrient withdrawal and chloroquine treatment induces oxidative stress-dependent mitochondrial depolarization resulting in mixed apoptotic and necrotic death of glioma cells.

Cytotoxicity of Chloroquine toward FCS-Deprived U251 Cells is Mediated by Interaction with Lysosomes

The analysis of intracellular acridine orange fluorescence demonstrated that FCS deprivation, but not chloroquine alone, induced accumulation of acidic vesicles, presumably autophagolysosomes, in the cytoplasm of U251 cells (Fig. 3a). The volume of intracellular acidic compartment in starved cells was further increased upon chloroquine addition in a time-dependent manner (Fig. 3a, b). This was associated with the appearance of large cytoplasmic vacuoles in serum-deprived cells starting from 4 h of the beginning of chloroquine treatment, as confirmed by both light and electron microscopy (Fig. 3c, d). Bafilomycin A1, a proton pump inhibitor known to inhibit lysosomal acidification and uptake of chloroquine into lysosomes (31,32), inhibited chloroquine-triggered intracytoplasmic accumulation of acidic vesicles (Fig. 3a) and vacuolization (Fig. 3c, d). Moreover, bafilomycin rescued starved glioma cells from the oxidative stress and ensuing cytotoxicity induced by chloroquine (Fig. 3e–g). Conversely, antioxidant agents N-acetylcysteine (4 mM) and butylated hydroxyanisole (200 μM) failed to affect chloroquine-mediated vacuolization and acidification (data not shown), indicating that these events preceded induction of oxidative stress. These data suggest that the cytotoxic effect of chloroquine against nutrient-deprived glioma cells is probably mediated by its interaction with the cellular lysosomal compartment.

AMPK Inhibition Contributes to Chloroquine Toxicity Toward Serum-Deprived U251 Cells

AMPK is a principal energy-sensing intracellular enzyme with major role in maintaining energy homeostasis and cell survival in energy deficient conditions (33). Accordingly, immunoblot analysis revealed that FCS deprivation induced activation of AMPK in U251 glioma cells (Fig. 4a). Chloroquine alone did not affect AMPK phosphorylation, but significantly suppressed AMPK activation induced by serum deprivation (Fig. 4a). The AMPK activator AICAR significantly reduced the cytotoxic effect of chloroquine in starved U251 cells (Fig. 4b). Moreover, shRNA-mediated AMPK inactivation mimicked the cytotoxic activity of chloroquine in nutrient-deprived glioma cells (Fig. 4c, d), thus confirming that it was at least partly mediated by AMPK inhibition.

Chloroquine is Toxic to Serum-Deprived L929 Fibrosarcoma and B16 Melanoma Cells

To eliminate possibility that the observed effects of chloroquine were limited to U251 glioma cells, we performed a similar set of experiments on L929 fibrosarcoma and B16 melanoma cells. In accordance with the results obtained in U251 cells, chloroquine in a dose-dependent manner potentiated the reduction in cell numbers and mitochondrial dehydrogenase activity in FCS-deprived L929 and B16 cells (Fig. 5a, b). The induction of oxidative stress (Fig. 5c), mitochondrial depolarization (Fig. 5d), intracellular acidification (Fig. 5e) and mixed apoptotic/necrotic death (Fig. 5f) were also observed in serum-deprived B16 cells. Moreover, chloroquine toxicity towards starved B16 cells was completely prevented by bafilomycin (Fig. 5g) and significantly

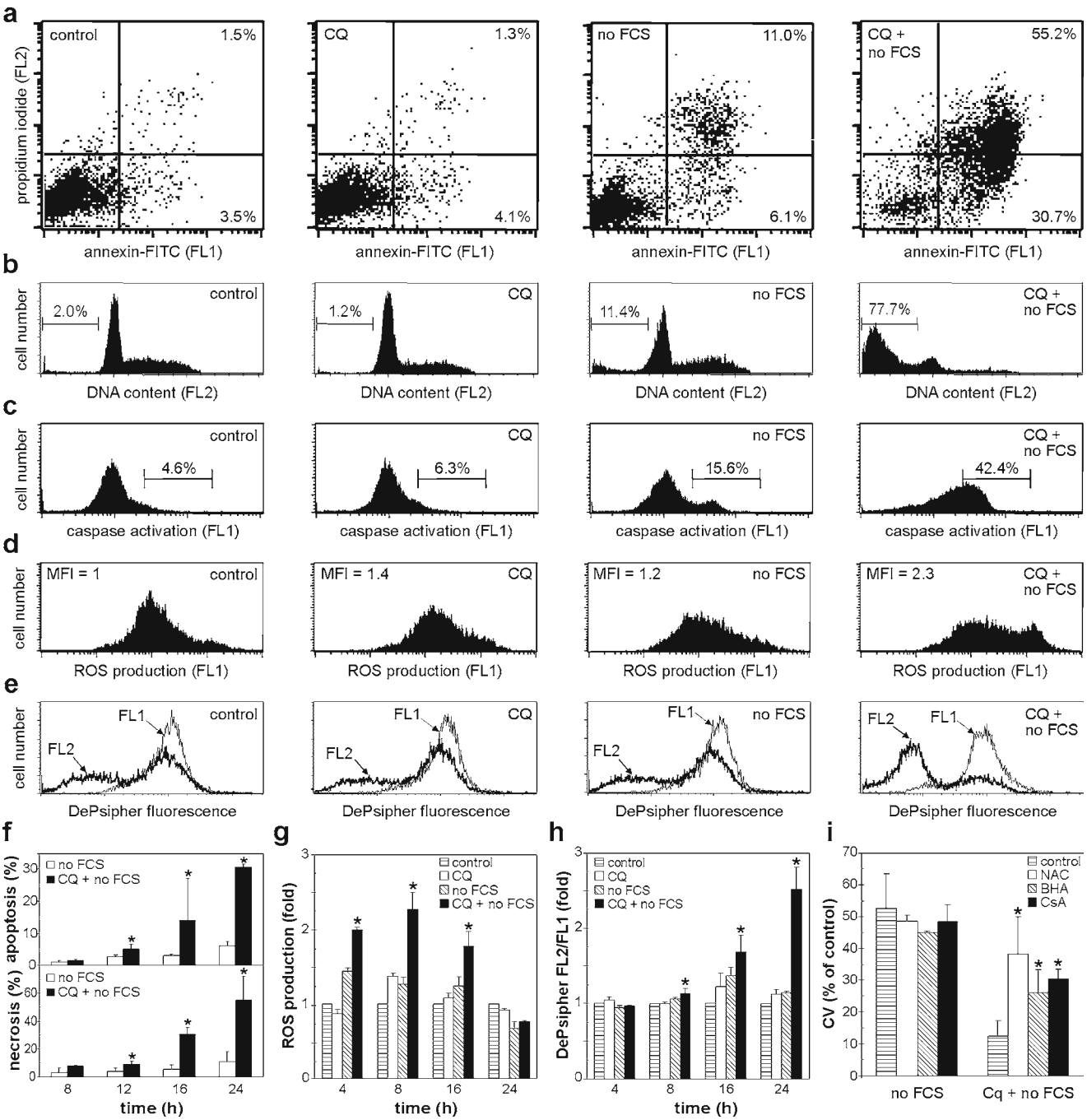

Fig. 2 Chloroquine induces oxidative stress- and mitochondrial depolarization-mediated apoptosis and necrosis in FCS-depleted cancer cells. (**a**–**h**) U251 cells were incubated in medium with or without FCS, in the absence or presence of chloroquine (CQ; 20 μM). (**a**, **f**) After 24 h (**a**) or at the indicated time points (**f**), the cells were stained with annexin-FITC/PI and the flow cytometric analysis of phosphatidylserine externalization (apoptosis) and membrane damage (necrosis) was performed. (**b**, **c**) After 24 h, the cells were stained with PI (**b**) or ApoStat (**c**) and the flow cytometric analysis of DNA fragmentation or caspase activation, respectively, was performed. (**d**, **g**) The production of ROS in DHR-stained cells was analyzed by flow cytometry after 8 h (**d**) or at the indicated time points (**g**). (**e**, **h**) Mitochondrial depolarization in DePsipher-cells was assessed by flow cytometry after 24 h (**e**) or at the indicated time points (**h**). (**i**) U251 cells were incubated in medium with FCS (control) or in FCS-depleted medium, in the absence or presence of chloroquine (20 μM) and/or N-acetylcysteine (NAC; 5 mM), butylated hydroxyanisole (BHA; 200 μM) or cyclosporine A (CsA; 1 μM). Cell viability was analyzed after 24 h using crystal violet (CV) test. Representative dot plots and histograms are presented (**a**–**e**). The data are mean ± SD values from three experiments (**f**–**h**) or mean ± SD values of triplicates from a representative of three experiments (**i**) [*$p < 0.05$ refers to cells incubated without FCS (**f**), cells incubated in FCS-deprived medium or treated with chloroquine (**g**, **h**), or cells treated with chloroquine in FCS-deprived medium (**i**)].

reduced by AICAR (Fig. 5h), thus confirming the involvement of lysosomal acidification and AMPK in chloroquine-mediated melanoma cell death. Similar results were obtained with L929 cells (data not shown). The ability of

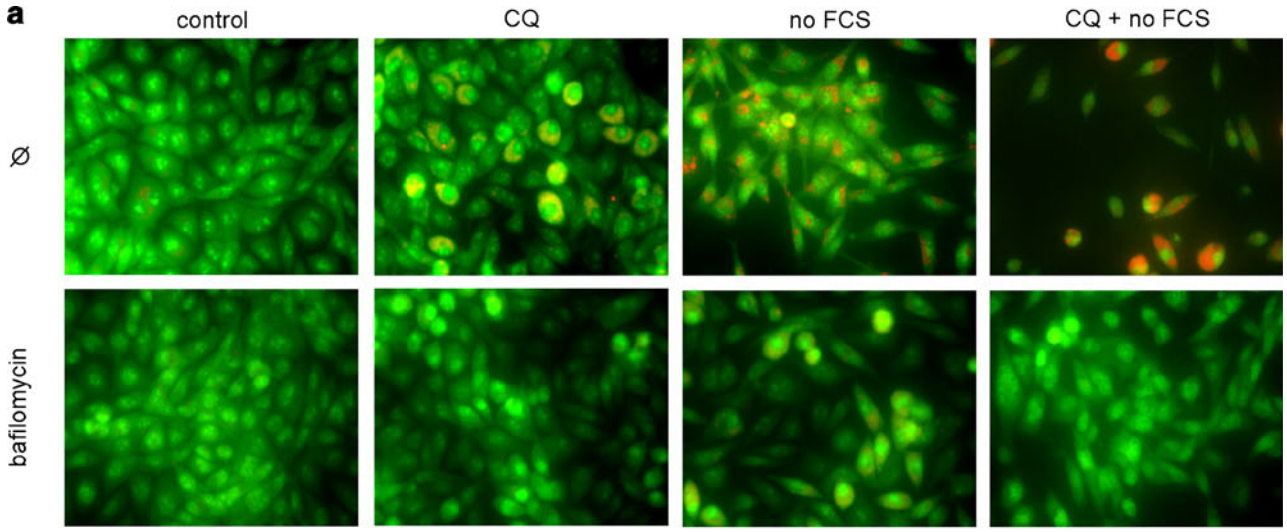
a
control
CQ
no FCS
CQ + no FCS
Ø
bafilomycin

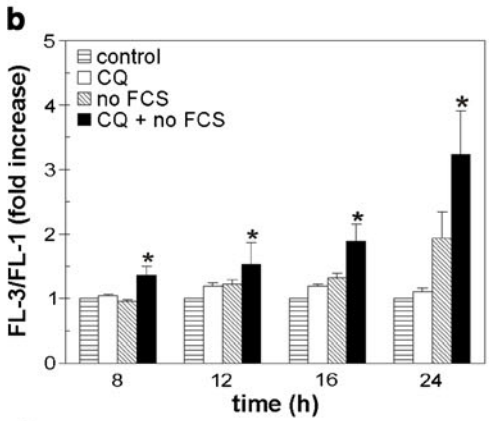
b
FL-3/FL-1 (fold increase)
control
CQ
no FCS
CQ + no FCS
time (h)

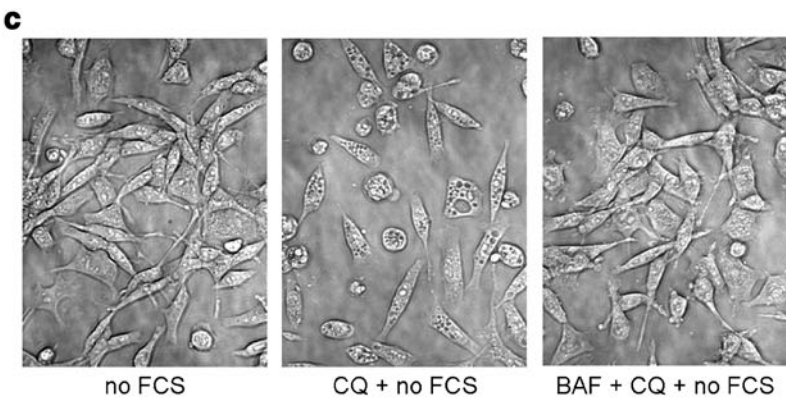
c
no FCS
CQ + no FCS
BAF + CQ + no FCS

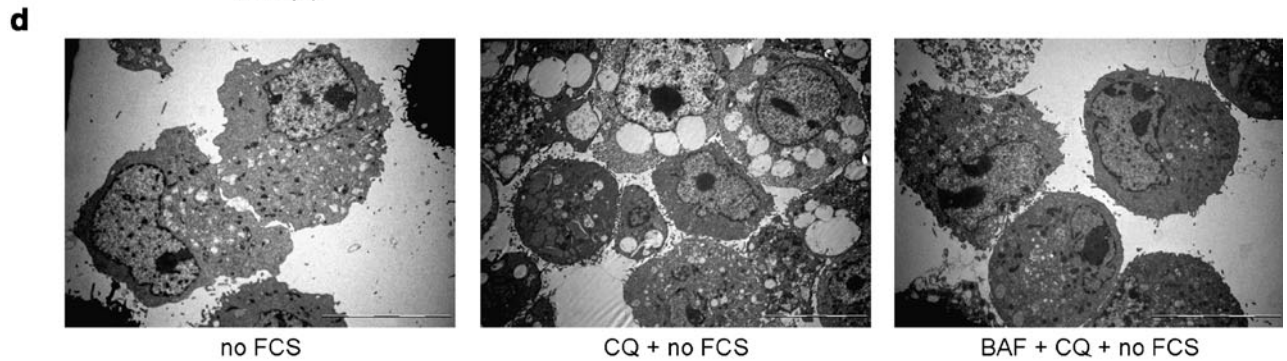
d
no FCS
CQ + no FCS
BAF + CQ + no FCS

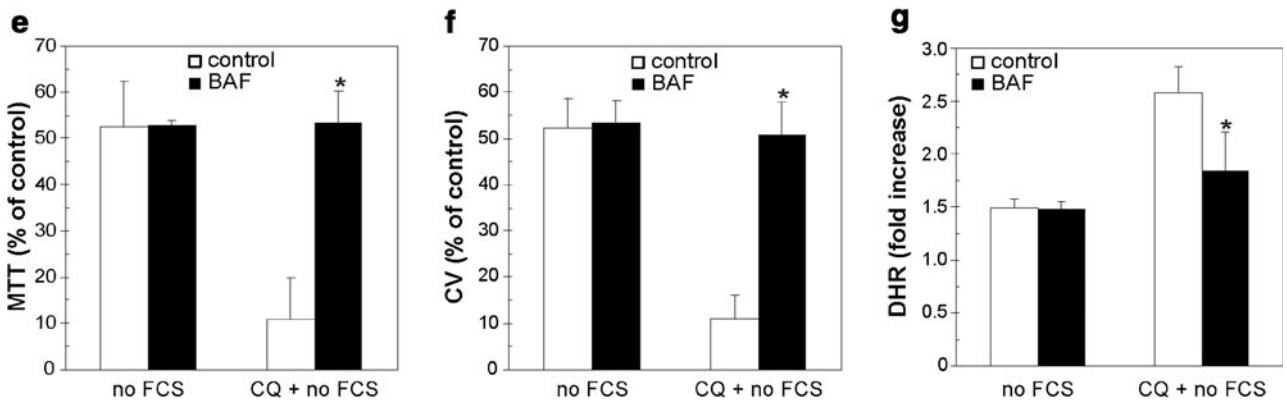
e
MTT (% of control)
control
BAF
no FCS
CQ + no FCS
f
CV (% of control)
control
BAF
no FCS
CQ + no FCS
g
DHR (fold increase)
control
BAF
no FCS
CQ + no FCS

Fig. 3 Cytotoxicity of chloroquine against FCS-deprived cancer cells depends on its interaction with lysosomes. (**a**, **b**) U251 cells were incubated in medium with or without FCS, in the absence or presence of chloroquine (CQ; 20 μM). The increase in acridine orange-stained intracellular acidic compartment was demonstrated by fluorescent microscopy after 24 h (**a**), or quantified by flow cytometry at the indicated time points (**b**). (**c**–**g**) U251 cells were incubated in FCS-free medium without or with chloroquine (20 μM) and bafilomycin A1 (BAF; 2 nM). Cell morphology was examined after 4 h by phase contrast (**c**) or electron microscopy (**d**), cell viability was determined after 24 h by MTT (**e**) or crystal violet (CV) test (**f**), and oxidative stress was assessed after 8 h by flow cytometric analysis of DHR-stained cells (**g**). The data are mean ± SD values from three separate experiments (**b**, **g**) or mean ± SD values of triplicates from a representative of three experiments (**e**, **f**) [*$p < 0.05$ refers to control cells (**b**) or starved cells treated with chloroquine alone (**e**–**g**)].

chloroquine to induce bafilomycin-preventable morphological changes and vacuolization of L929 and B16 cells incubated in serum-free medium was confirmed by light microscopy (Fig. 5i).

Chloroquine Potentiates Antimelanoma Effect of Calorie Restriction *In Vivo*

Finally, we investigated the possible therapeutic usefulness of combined treatment with calorie restriction and chloroquine in a mouse melanoma model. Calorie restriction significantly reduced the weight of animals (16.0±0.8 g and 14.7±0.7 g in groups without and with chloroquine, respectively) in comparison to normally fed animals (21.4±3.0 g and 21.9±1.4 g in control and chloroquine group, respectively) at the end of the experiment. Daily measurement of tumor size showed that both chloroquine and calorie restriction alone inhibited melanoma growth to some extent (Fig. 6a). However, in animals exposed to combination of caloric restriction and i.p. chloroquine, the tumors were not palpable until 2 days before the end of experiment (Fig. 6a), and the average weight of excised tumors was significantly lower in comparison with other three groups (control, calorie restriction alone and chloroquine alone) (Fig. 6b). Representative tumors from all experimental groups were presented in Fig. 6d. Electron microscopy analysis of tumors demonstrated necrosis (N) in both calorie restricted and chloroquine-treated group, but the necrotic changes were clearly most prominent in tumors of animals receiving combined treatment (Fig. 6c, upper panel). Mitochondrial swelling (MS), observed in tumors from calorie restricted mice, progressed to an almost complete disintegration (MD) in melanoma cells from animals exposed to combined treatment (Fig. 6d, lower panel). In addition to increased number of lysosomes (L), the accumulation of lipid

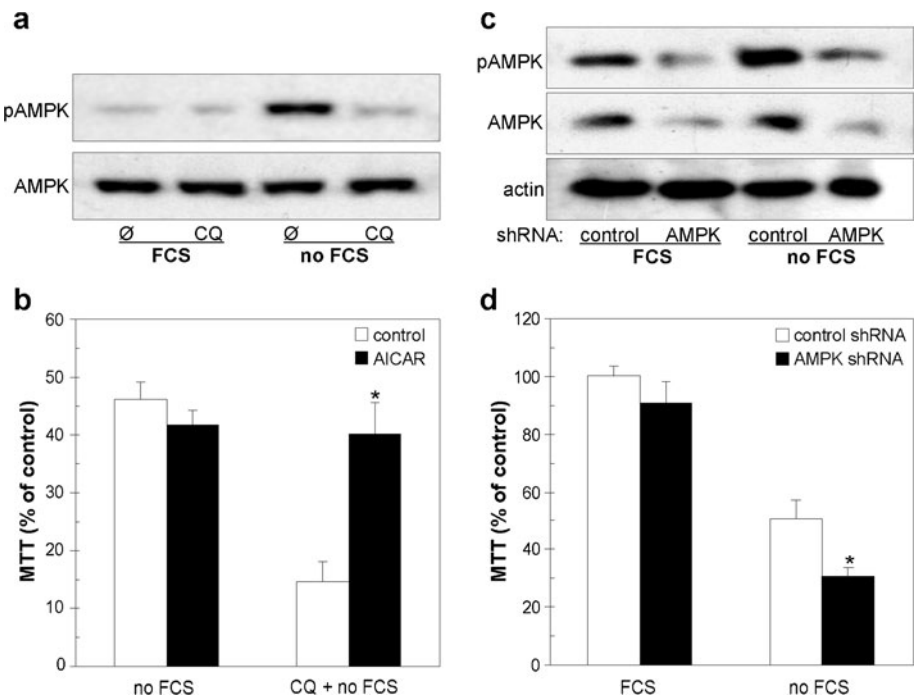

Fig. 4 AMPK inhibition is involved in anticancer activity of chloroquine against FCS-depleted cells. (**a**) U251 cells were incubated in medium with or without FCS, in the absence or presence of chloroquine (CQ; 20 μM), and immunoblot analysis of phosphorylated and total AMPK was performed after 4 h. (**b**) FCS-depleted U251 cells were incubated without or with chloroquine (20 μM) and/or AICAR (250 μM), and cell viability was assessed after 24 h by MTT test. The data are mean ± SD values of triplicates from a representative of three experiments (*$p < 0.05$ refers to starved cells treated with chloroquine alone). (**c**) Immunoblot confirmation of shRNA-mediated AMPK knockdown in U251 cells. (**d**) U251 cells transfected with control or AMPK shRNA were incubated in medium with or without FCS, and cell viability was determined after 24 h by MTT assay. The data are mean ± SD values of triplicates from a representative of three experiments (*$p < 0.05$ refers to control shRNA-transfected cells in medium without FCS).

droplets (LD) was clearly detectable in melanoma tumors of calorie restricted animals treated with chloroquine (Fig. 6d, lower panel). Lipid accumulation in melanoma tissue of these animals was confirmed by Sudan black B staining (Fig. 6e, upper panel). Hematoxylin and eosin staining demonstrated the presence of massive necrosis in melanoma tissue (Fig. 6e, lower panel), but not in kidneys, livers, spleens and hearts of animals exposed to both caloric restriction and chloroquine (Fig. 6f). These results indicate that chloroquine-mediated suppression of melanoma growth in calorie restricted animals is associated with mitochondrial damage, lysosomal and lipid accumulation and necrotic melanoma cell death.

DISCUSSION

The present study demonstrates that chloroquine exerts strong anticancer activity against nutrient-deprived cancer cells, both *in vitro* and *in vivo*. The observed effect, at least *in vitro*, did not exclusively depend on inhibition of autophagy and involved lysosome accumulation and subsequent induction of oxidative stress, mitochondrial depolarization and AMPK inhibition, resulting in mixed apoptotic/necrotic death of cancer cells (Fig. 7).

In accordance with previous reports (34), chloroquine in our study efficiently suppressed autophagic proteolysis in serum-starved cancer cells, as confirmed by an increase in levels of LC3-II and p62, which are both degraded within autophagolysosomes (28). Somewhat surprisingly, other autophagy inhibitors failed to mimic rapid chloroquine-mediated killing of nutrient-restricted cancer cells, despite efficient reduction of intracellular acidification. Their cytotoxic effect, as well as that of the LC3b knockdown, was delayed in comparison with chloroquine, indicating that the inhibition of autophagy was not solely responsible for the chloroquine-mediated anticancer effect. Our results are in agreement with very recent findings of Maycotte *et al.*, demonstrating that chloroquine sensitizes breast cancer cells to autophagy-inducing chemotherapeutics independently of autophagy inhibition (35). Moreover, bafilomycin A1, a proton pump blocker that potently inhibits lysosomal acidification and subsequent proteolytic digestion (30), completely prevented chloroquine toxicity toward serum-deprived cancer cells, thus confirming that it was not dependent on blockade of autophagic proteolysis. A more plausible mechanism might involve a direct chloroquine interaction with the cellular lysosomal compartment. Namely, in contrast to other autophagy inhibitors, chloroquine in our study increased intracellular accumulation of acidic vesicles, presumably lysosomes, and caused extensive vacuolization, both of which were prevented by inhibiting lysosomal acidification with bafilomycin. These data confirm previous observations that chloroquine increases accumulation of lysosomes, while blocking their fusion with autophagosomes in serum-deprived cancer cells (34). In its unprotonated form chloroquine can diffuse freely across the membranes of the cells and organelles, but once protonated, it becomes "trapped" in the acidic organelles such as the lysosomes, which leads to the increase of lysosomal volume and inhibition of their proteolytic enzymes (20). Bafilomycin-mediated blockade of chloroquine's effect on lysosomal compartment and ensuing cytotoxicity has recently been described in serum-rich cultures of retinal cells (36), and the lysosomal disruption has been proposed responsible for the toxicity of chloroquine to hepatocytes (37). However, to the best of our knowledge, the present study is the first to demonstrate that a similar mechanism might be operational in nutrient-deficient cancer cells. It should be noted that chloroquine at high concentrations was able to kill cancer cells even in the absence of nutrient deprivation (12–17). However, at lower concentrations (20 μM and less), it induced only moderate and transient vacuolization of cells cultivated in nutrient-rich medium, indicating that nutrient deprivation somehow increased sensitivity of cancer cells to chloroquine-induced lysosomal dilatation and ensuing cell death.

Chloroquine-mediated lysosomal dysfunction in serum-deprived cancer cells resulted in oxidative stress and subsequent mitochondrial depolarization, ultimately culminating in caspase activation and mixed apoptotic/necrotic cell death. These data concord with the recent findings that chloroquine induces apoptosis associated with mitochondrial membrane depolarization and activation of caspases in breast cancer cells (38). Having in mind that oxidative stress could cause mitochondrial permeability transition pore opening and mitochondrial depolarization, leading to release of cytohrome c from mitochondria and subsequent activation of caspase

Fig. 5 Chloroquine is toxic to serum-deprived L929 and B16 cells. (**a**, **b**) L929 (**a**) and B16 cells (**b**) were incubated in medium with or without FCS, in the absence or presence of different concentrations of chloroquine (CQ) and cell viability was assessed after 24 h by MTT or crystal violet (CV) test. Data are mean ± SD values of triplicates from a representative of three experiments (*$p < 0.05$ refers to FCS-deprived cells without chloroquine). (**c**–**f**) B16 cells were incubated in medium with or without FCS, in the absence or presence of chloroquine (20 μM). (**c**) The flow cytometric analysis of ROS production in DHR stained cells was performed after 8 h. (**d**–**f**) Mitochondrial depolarization in DePsipher-stained cells (**d**), intracellular acidification in acridine orange-stained cells (**e**), or phosphatidylserine externalization/membrane damage in cells stained with annexin-FITC/PI (**f**) was performed after 24 h by flow cytometry. (**c**–**f**) The data are mean ± SD values from three independent experiments (*$p < 0.05$ refers to FCS-deprived cells without chloroquine). (**g**, **h**) FCS-depleted B16 cells were incubated without or with chloroquine (20 μM), in the absence or presence of bafilomycin A1 (BAF; 2 nM) (**g**) or AICAR (250 μM) (**h**), and cell viability was assessed after 24 h by crystal violet (CV) staining. Data are presented as mean ± SD values of triplicates from a representative of three experiments (*$p < 0.05$ refers to starved cells treated with chloroquine alone). (**i**) Cell morphology of FCS-depleted B16 and L929 cells incubated without or with chloroquine (20 μM) in the absence or presence of bafilomycin (2 nM) was examined by phase contrast microscopy.

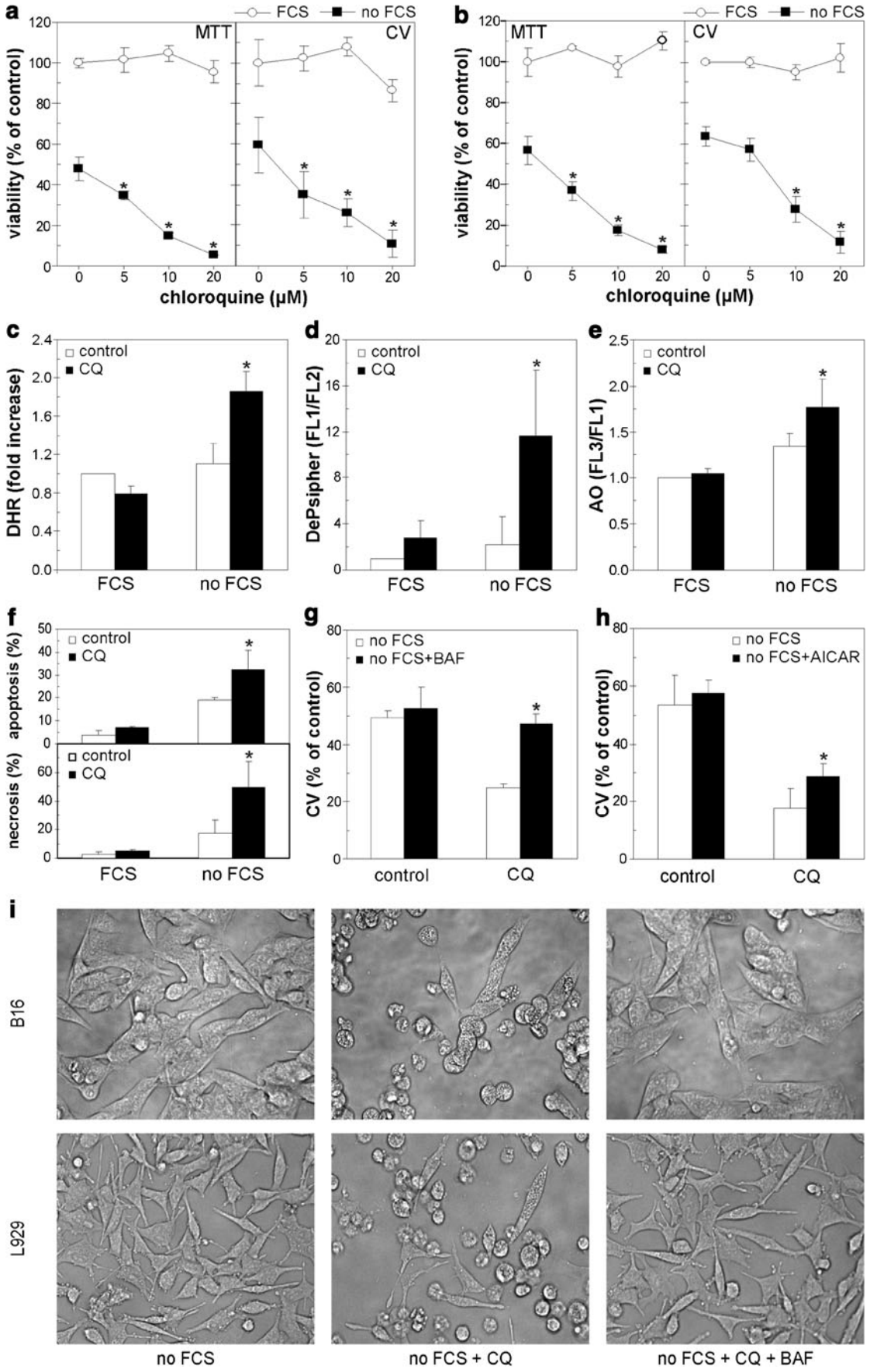
a
FCS
no FCS
MTT
CV
viability (% of control)
chloroquine (μM)
b
c
DHR (fold increase)
control
CQ
d
DePsipher (FL1/FL2)
e
AO (FL3/FL1)
f
apoptosis (%)
necrosis (%)
g
no FCS
no FCS+BAF
CV (% of control)
h
no FCS+AICAR
i
B16
L929
no FCS
no FCS + CQ
no FCS + CQ + BAF

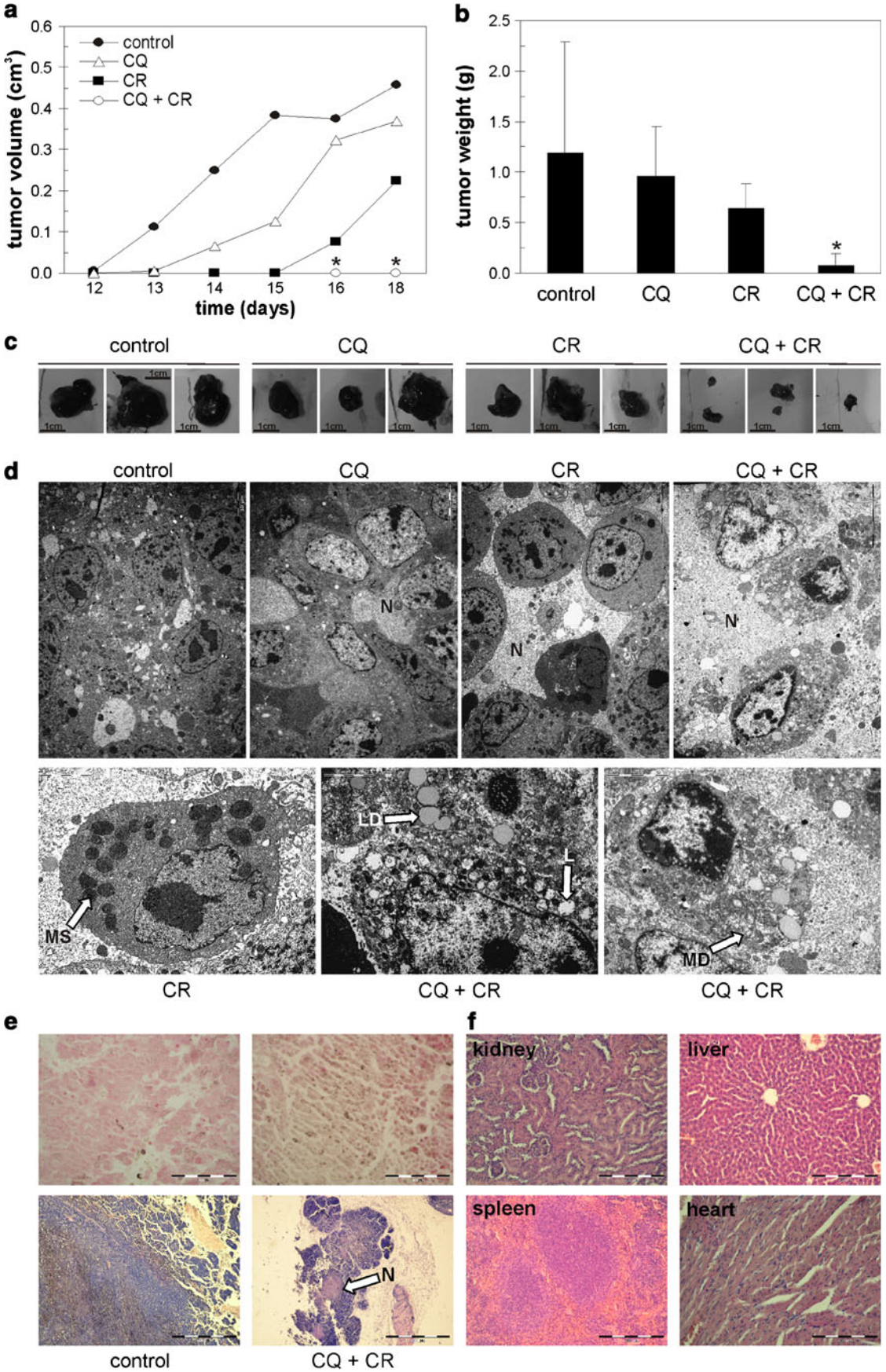
a
tumor volume (cm³)
control
CQ
CR
CQ + CR
time (days)
b
tumor weight (g)
control
CQ
CR
CQ + CR
c
control
CQ
CR
CQ + CR
d
control
CQ
CR
CQ + CR
N
MS
LD
L
MD
CR
CQ + CR
CQ + CR
e
control
CQ + CR
N
f
kidney
liver
spleen
heart

◀ **Fig. 6** Chloroquine potentiates antimelanoma effect of calorie restriction *in vivo*. (**a**–**e**) Five days after s.c. injection of B16 melanoma cells (3×10^5 cells/mouse), chloroquine (CQ) in PBS (20 mg/kg b.w./day) or PBS alone were administered daily (i.p.) to normally fed or calorie-restricted (CR) mice ($n=8$ per each group). (**a**) The tumor volumes were measured at different time points after the challenge. (**b**, **c**) The tumor weights were measured at autopsy after 20 days (**b**) and representative tumors were photographed (**c**). (**a**, **b**) Data are presented as mean ± SD values (*$p <$ 0.05 refers to all other groups; SD values in (**a**) were omitted for clarity). (**d**) The electronic microscopy of tumor tissues: N - necrosis, MS - mitochondrial swelling, MD - mitochondrial disintegration, LD - lipid droplets, L - lysosomes; scale bar 10 μM (upper panel) and 5 μM (lower panel). (**e**) Sudan staining (upper panel; scale bar 100 μM) and hematoxylin & eosin staining (lower panel, scale bar 1000 μM)) of tumor tissues from control and chloroquine + calorie restricted mice: N - necrosis. (**f**) Hematoxylin & eosin staining of normal tissues from calorie restricted mice treated with chloroquine (scale bar 200 μM).

cascades (39,40), we propose a similar mechanism for chloroquine-induced killing of nutrient-deprived tumor cells. Lysosomal dilatation, oxidative stress and mitochondrial damage are common events in both apoptosis and necrosis (41,42), which is consistent with the ability of chloroquine to induce necrosis in lung cancer cells (12) and mixed apoptotic/necrotic death of starved tumor cells in the present study. In accordance with the protective role of the intracellular energy-sensing enzyme AMPK in metabolic stress (33), its inhibition by chloroquine was apparently involved in apoptotic/necrotic death of nutrient deprived cancer cells. It should be noted, however, that pharmacological activation or shRNA-mediated suppression of AMPK failed to affect or mimic, respectively, chloroquine-triggered vacuolization and acidification in serum-deprived U251 cells (unpublished observation), indicating that AMPK inhibition by chloroquine occurred independently or downstream of its interference with the lysosomal compartment (Fig. 7). We are currently investigating possible connections between lysosomal accumulation-dependent oxidative stress and AMPK inactivation in nutrient-deprived melanoma cells exposed to chloroquine.

While confirming previous findings on moderate efficiency of calorie restriction or chloroquine alone in B16 mouse melanoma model (43,44), we have demonstrated that combination of calorie restriction and chloroquine almost completely abolished B16 melanoma growth *in vivo*. In accordance with the *in vitro* results, electron microscopy revealed lysosomal accumulation and massive tumor necrosis upon combined treatment, while calorie restriction-induced mitochondrial swelling progressed to a complete mitochondrial disintegration in melanoma tissue of mice exposed to both calorie restriction and chloroquine. Interestingly, a large amount of lipid droplets was also observed in tumors of animals exposed to the combination treatment, implying that energy metabolism in melanoma cells of these animals was completely disturbed. Even though it seems paradoxical that energy-deprived tumors accumulate lipid droplets, this could be explained by the fact that lipids are usually degraded in lysosomes, which were damaged by combined treatment of chloroquine and starvation. Accordingly, large vacuoles resembling lysosomes and numerous lipid droplets were seen by electronic microscopy of tissue samples taken from patients with lysosomal storage disorders (45), who are unable to metabolize lipids because of lysosomal dysfunction. The accumulation of lipid droplets could also result from inhibition of AMPK, which blocks lipid catabolism (46). Having in mind that chloroquine also inhibits glutamate dehydrogenase (47), a mitochondrial enzyme necessary for ATP production under energy-deficient conditions (48), it would be interesting to investigate if this effect is involved in synergistic anticancer action of chloroquine and nutrient deprivation. Finally, it seems plausible to assume that inhibition of autophagy could contribute to chloroquine-mediated potentiation of the anti-cancer effect

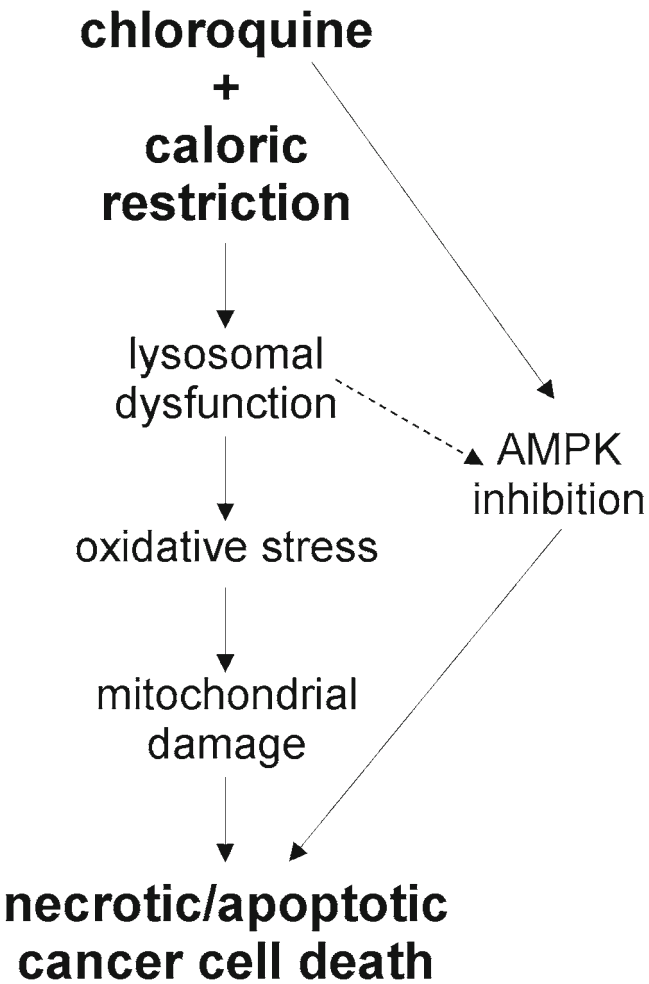

Fig. 7 A hypothetical model of the intracellular mechanisms underlying synergistic anticancer effect of chloroquine and caloric restriction. Chloroquine induces mixed apoptotic and necrotic death of tumor cells mediated by lysosomal damage, oxidative stress and mitochondrial depolarization. Chloroquine-mediated inhibition of starvation-induced AMPK activity contributes to its anticancer effect independently or as a consequence of lysosomal damage (*dashed line*).

of calorie restriction *in vivo*. Indeed, a recent study, published while the present manuscript was in preparation, indicated that the autophagy inhibition by chloroquine could contribute to its synergistic cooperation with leucine deprivation in restricting human melanoma growth in a mice xenograft model (49). However, as we only sporadically observed autophagosomes/autophagolysosomes in melanoma tissue irrespectively of treatment modality, this issue remains to be investigated further.

In conclusion, the present study demonstrates the *in vitro* and *in vivo* potentiation of calorie restriction-induced anticancer effect by chloroquine, probably mediated by lysosomal dysfunction-associated oxidative stress leading to mitochondrial damage and apoptotic/necrotic death of tumor cells. The risk of potential chloroquine toxicity is greatly reduced by using the drug at concentration (20 mg/kg) much lower than clinically-used doses (18), combined with calorie restriction which is more devastating to cancer cells than to their normal counterparts. The absence of toxicity to normal tissues observed in our study could also be explained by chloroquine affinity towards more acidic tumor tissues, as well as melanin (44). Having in mind that chloroquine is already in many anticancer clinical trials (http://www.clinicaltrials.gov) and that its approval for treatment of malaria and autoimmune disorders could enable an easy, fast and inexpensive "repurposing", our data support further investigation of calorie restriction-chloroquine combination in cancer therapy.

ACKNOWLEDGMENTS & DISCLOSURES

The study was supported by the Ministry of Science and Technological Development of the Republic of Serbia (grants 173053 to LHT and 41025 to VT). Ljubica Harhaji-Trajkovic is a recipient of the UNESCO L'OREAL national scholarship program "For Women in Science" (contract number 403F). The authors declare that there are no conflicts of interest.

REFERENCES

1. Kennedy BK, Steffen KK, Kaeberlein M. Ruminations on dietary restriction and aging. Cell Mol Life Sci. 2007;64:1323–8.
2. Omodei D, Fontana L. Calorie restriction and prevention of age-associated chronic disease. FEBS Lett. 2011;585:1537–42.
3. Grifantini K. Understanding pathways of calorie restriction: a way to prevent cancer? J Natl Cancer Inst. 2008;100:619–21.
4. Longo VD, Fontana L. Calorie restriction and cancer prevention: metabolic and molecular mechanisms. Trends Pharmacol Sci. 2010;31:89–98.
5. Yorimitsu T, Klionsky DJ. Autophagy: molecular machinery for self-eating. Cell Death Differ. 2005;12 Suppl 2:1542–52.
6. Mizushima N, Levine B, Cuervo AM, Klionsky DJ. Autophagy fights disease through cellular self-digestion. Nature. 2008;451:1069–75.
7. Gump JM, Thorburn A. Autophagy and apoptosis: what is the connection? Trends Cell Biol. 2011;21:387–92.
8. Thorburn A. Apoptosis and autophagy: regulatory connections between two supposedly different processes. Apoptosis. 2008;13:1–9.
9. Warburg O. On the origin of cancer cells. Science. 1956;123:309–14.
10. Levy JM, Thorburn A. Targeting autophagy during cancer therapy to improve clinical outcomes. Pharmacol Ther. 2011;131:130–41.
11. Maycotte P, Thorburn A. Autophagy and cancer therapy. Cancer Biol Ther. 2011;11:127–37.
12. Fan C, Wang W, Zhao B, Zhang S, Miao J. Chloroquine inhibits cell growth and induces cell death in A549 lung cancer cells. Bioorg Med Chem. 2006;14:3218–22.
13. Jiang PD, Zhao YL, Deng XQ, Mao YQ, Shi W, Tang QQ, *et al.* Antitumor and antimetastatic activities of chloroquine diphosphate in a murine model of breast cancer. Biomed Pharmacother. 2010;64:609–14.
14. Munshi A. Chloroquine in glioblastoma–new horizons for an old drug. Cancer. 2009;115:2380–3.
15. Rahim R, Strobl JS. Hydroxychloroquine, chloroquine, and all-trans retinoic acid regulate growth, survival, and histone acetylation in breast cancer cells. Anticancer Drugs. 2009;20:736–45.
16. Solomon VR, Hu C, Lee H. Design and synthesis of chloroquine analogs with anti-breast cancer property. Eur J Med Chem. 2010;45:3916–23.
17. Zheng Y, Zhao YL, Deng X, Yang S, Mao Y, Li Z, *et al.* Chloroquine inhibits colon cancer cell growth *in vitro* and tumor growth *in vivo* via induction of apoptosis. Cancer Invest. 2009;27:286–92.
18. Hu C, Solomon VR, Ulibarri G, Lee H. The efficacy and selectivity of tumor cell killing by Akt inhibitors are substantially increased by chloroquine. Bioorg Med Chem. 2008;16:7888–93.
19. Solomon VR, Lee H. Chloroquine and its analogs: a new promise of an old drug for effective and safe cancer therapies. Eur J Pharmacol. 2009;625:220–33.
20. Poole B, Ohkuma S. Effect of weak bases on the intralysosomal pH in mouse peritoneal macrophages. J Cell Biol. 1981;90:665–9.
21. Glaumann H, Ahlberg J. Comparison of different autophagic vacuoles with regard to ultrastructure, enzymatic composition, and degradation capacity–formation of crinosomes. Exp Mol Pathol. 1987;47:346–62.
22. Lum JJ, Bauer DE, Kong M, Harris MH, Li C, Lindsten T, *et al.* Growth factor regulation of autophagy and cell survival in the absence of apoptosis. Cell. 2005;120:237–48.
23. Carew JS, Medina EC, Esquivel 2nd JA, Mahalingam D, Swords R, Kelly K, *et al.* Autophagy inhibition enhances vorinostat-induced apoptosis via ubiquitinated protein accumulation. J Cell Mol Med. 2010;14:2448–59.
24. Kaludjerovic GN, Miljkovic D, Momcilovic M, Djinovic VM, Mostarica Stojkovic M, Sabo TJ, *et al.* Novel platinum(IV) complexes induce rapid tumor cell death *in vitro*. Int J Cancer. 2005;116:479–86.
25. Harhaji L, Isakovic A, Vucicevic L, Janjetovic K, Misirkic M, Markovic Z, *et al.* Modulation of tumor necrosis factor-mediated cell death by fullerenes. Pharm Res. 2008;25:1365–76.
26. Bastien-Dionne PO, Valenti L, Kon N, Gu W, Buteau J. Glucagon-like peptide 1 inhibits the sirtuin deacetylase SirT1 to stimulate pancreatic beta-cell mass expansion. Diabetes. 2011;60:3217–22.
27. Kaushik S, Rodriguez-Navarro JA, Arias E, Kiffin R, Sahu S, Schwartz GJ, *et al.* Autophagy in hypothalamic AgRP neurons regulates food intake and energy balance. Cell Metab. 2011;14:173–83.

28. Bjorkoy G, Lamark T, Brech A, Outzen H, Perander M, Overvatn A, *et al.* p62/SQSTM1 forms protein aggregates degraded by autophagy and has a protective effect on huntingtin-induced cell death. J Cell Biol. 2005;171:603–14.
29. Blommaart EF, Krause U, Schellens JP, Vreeling-Sindelarova H, Meijer AJ. The phosphatidylinositol 3-kinase inhibitors wortmannin and LY294002 inhibit autophagy in isolated rat hepatocytes. Eur J Biochem. 1997;243:240–6.
30. Klionsky DJ, Elazar Z, Seglen PO, Rubinsztein DC. Does bafilomycin A1 block the fusion of autophagosomes with lysosomes? Autophagy. 2008;4:849–950.
31. Rogers SW, Rechsteiner M. Degradation of structurally characterized proteins injected into HeLa cells. Effects of intracellular location and the involvement of lysosomes. J Biol Chem. 1988; 263:19843–9.
32. van Es HH, Renkema H, Aerts H, Schurr E. Enhanced lysosomal acidification leads to increased chloroquine accumulation in CHO cells expressing the pfmdr1 gene. Mol Biochem Parasitol. 1994;68:209–19.
33. Hardie DG, Hawley SA, Scott JW. AMP-activated protein kinase - development of the energy sensor concept. J Physiol. 2006;574:7–15.
34. Boya P, Gonzalez-Polo RA, Casares N, Perfettini JL, Dessen P, Larochette N, *et al.* Inhibition of macroautophagy triggers apoptosis. Mol Cell Biol. 2005;25:1025–40.
35. Maycotte P, Aryal S, Cummings CT, Thorburn J, Morgan MJ, Thorburn A. Chloroquine sensitizes breast cancer cells to chemotherapy independent of autophagy. Autophagy. 2012;8:200–12.
36. Yoon YH, Cho KS, Hwang JJ, Lee SJ, Choi JA, Koh JY. Induction of lysosomal dilatation, arrested autophagy, and cell death by chloroquine in cultured ARPE-19 cells. Invest Ophthalmol Vis Sci. 2010;51:6030–7.
37. Michihara A, Toda K, Kubo T, Fujiwara Y, Akasaki K, Tsuji H. Disruptive effect of chloroquine on lysosomes in cultured rat hepatocytes. Biol Pharm Bull. 2005;28:947–51.
38. Jiang PD, Zhao YL, Shi W, Deng XQ, Xie G, Mao YQ, *et al.* Cell growth inhibition, G2/M cell cycle arrest, and apoptosis induced by chloroquine in human breast cancer cell line Bcap-37. Cell Physiol Biochem. 2008;22:431–40.
39. Loeffler M, Kroemer G. The mitochondrion in cell death control: certainties and incognita. Exp Cell Res. 2000;256:19–26.
40. Zorov DB, Juhaszova M, Sollott SJ. Mitochondrial ROS-induced ROS release: an update and review. Biochim Biophys Acta. 2006;1757:509–17.
41. Kim JS, He L, Lemasters JJ. Mitochondrial permeability transition: a common pathway to necrosis and apoptosis. Biochem Biophys Res Commun. 2003;304:463–70.
42. Ono K, Wang X, Han J. Resistance to tumor necrosis factor-induced cell death mediated by PMCA4 deficiency. Mol Cell Biol. 2001;21:8276–88.
43. Ershler WB, Berman E, Moore AL. Slower B16 melanoma growth but greater pulmonary colonization in calorie-restricted mice. J Natl Cancer Inst. 1986;76:81–5.
44. Inoue S, Hasegawa K, Ito S, Wakamatsu K, Fujita K. Antimelanoma activity of chloroquine, an antimalarial agent with high affinity for melanin. Pigment Cell Res. 1993;6:354–8.
45. Vogler C, Rosenberg HS, Williams JC, Butler I. Electron microscopy in the diagnosis of lysosomal storage diseases. Am J Med Genet Suppl. 1987;3:243–55.
46. Lin CL, Huang HC, Lin JK. Theaflavins attenuate hepatic lipid accumulation through activating AMPK in human HepG2 cells. J Lipid Res. 2007;48:2334–43.
47. Jarzyna R, Lenarcik E, Bryla J. Chloroquine is a potent inhibitor of glutamate dehydrogenase in liver and kidney-cortex of rabbit. Pharmacol Res. 1997;35:79–84.
48. Mastorodemos V, Zaganas I, Spanaki C, Bessa M, Plaitakis A. Molecular basis of human glutamate dehydrogenase regulation under changing energy demands. J Neurosci Res. 2005;79:65–73.
49. Sheen JH, Zoncu R, Kim D, Sabatini DM. Defective regulation of autophagy upon leucine deprivation reveals a targetable liability of human melanoma cells *in vitro* and *in vivo*. Cancer Cell. 2011;19:613–28.